Dispersive Spectrometry At Terahertz Frequencies for Probing the Quality of NbTiN Superconducting Films

A. Khudchenko, B. N. R. Lap, K. I. Rudakov, R. Hesper, V. P. Koshelets, *Member, IEEE*, P. N. Dmitriev, A. Chekushkin, F. V. Khan, E. S. Zhukova, L. S. Kadyrov, B. P. Gorshunov, and A. M. Baryshev

(Invited Paper)

***Abstract*—We present the quality measurements of thick (thicker than London penetration depth) NbTiN superconducting films at Terahertz frequencies using a Dispersive Fourier Transform Spectrometer (DFTS). The reflected RF signal from the tested film was measured in time domain, allowing us to separate it from other reflections. The complex conductivity of the film depends on frequency and determines the reflection coefficient. By comparing the film reflection in superconducting state (film temperature below Tc) with that of the normal state (film temperature above Tc), we characterized the film quality at terahertz frequencies, and directly probed the energy of the superconducting gap of the tested film. The experimental results were fitted using the extended Mattis-Bardeen theory and th obtained film parameters show a good agreement with the literature. In addition to the DFTS, we have also measured the properties of NbTiN film using Time Domain Spectroscopy (TDS). It is shown that both TDS and DFTS provide similar results, and both techniques can be used for the quality control of thick NbTiN films. The superconducting gap determined from the measurements by both DFTS and TDS are in good agreement for both solid and meshed films showing that there is no remarkable degradation in the film quality due to technological processes of lift-off or ion etching.**

***Index Terms*—Fourier transform spectrometer, superconductivity, terahertz spectrometry, thin films, time domain spectroscopy.**

Manuscript received October 3, 2021; revised January 4, 2022; accepted January 24, 2022. Date of publication February 1, 2022; date of current version March 1, 2022. This work was supported in part by Netherlands Academy of Science (NWO) grant "NWO-FAPESP Advanced Instrumentation for Astronomy" under Project 629.004.00, and in part by the Russian Foundation for Basic Research under Project 19-52-80023. The equipment of USU "Cryointegral" was used to carry out the research, USU was supported by the Ministry of Science and Higher Education of Russian Federation under Grant 075-15-2021-667. *(Corresponding author: Andrey Khudchenko.)*

A. Khudchenko and V. P. Koshelets are with the Astro Space Center, P.N. Lebedev Physical Institute, Moscow 119991, Russia (e-mail: khudchenko@asc.rssi.ru; valery@hitech.cplire.ru).

B. N. R. Lap is with the Kapteyn Astronomical Institute, University of Groningen, 9747 AD Groningen, The Netherlands, and also with The Netherlands Institute for Space Research, 9747 AD Groningen, The Netherlands (e-mail: b.lap@sron.nl).

K. I. Rudakov, R. Hesper, and A. M. Baryshev are with the Kapteyn Astronomical Institute, University of Groningen, 9747 AD Groningen, The Netherlands (e-mail: r.hesper@astro.rug.nl; a.m.baryshev@astro.rug.nl).

P. N. Dmitriev, A. Chekushkin, and F. V. Khan are with the Kotel'nikov Institute of Radioengineering and Electronics RAS, Moscow 125009, Russia.

E. S. Zhukova, L. S. Kadyrov, and B. P. Gorshunov are with the Moscow Institute of Physics and Technology, Dolgoprudny 141700 Moscow, Russia.

Color versions of one or more figures in this article are available at https://doi.org/10.1109/TASC.2022.3147736.

Digital Object Identifier 10.1109/TASC.2022.3147736

I. Introduction

SUPERCONDUCTOR-insulator-superconductor (SIS) mixers are known to be the most sensitive coherent detectors in the range 100–1300 GHz [1]–[3]. Heterodyne receivers based on these mixer are widely used in current mm and sub-mm radio observatories like HERSHEL satellite [3], and ground-based interferometers such as ALMA [4], NOEMA [5] and many others [6]–[8]. SIS receivers will also be used for future space telescope Millimetron [9] and ground-based facilities Suffa [10], AtLast [11], LLAMA [12]. The unique sensitivity of the SIS mixers is based on their quantum mixing properties [13] and on low-loss superconducting embedding circuits. For mixers operating at 100-700 GHz, the embedding micro-strip lines are commonly made out of Nb [1], [2]. Though, for the higher frequencies, the photon energy starts breaking Cooper-pairs in this material, resulting in extra resisting losses. Here, the superconductors with highest superconducting energy gap should be used. It was found that the most suitable material for the embedding circuit of SIS mixers operating in the frequency range 700- 1200 GHz was NbTiN, which was used as a bottom electrode material in state-of-the-art SIS mixers developed for different telescopes [3], [14]–[16].

In Fig. 1 one can see the cross-section of the SIS mixer operating at 800-950 GHz [16]. The Nb, AlN and NbN layers form the SIS junction, and the NbTiN with the Al acts as both the bottom and top electrodes of the embedding circuit. The top electrode manufactured out of Al has more losses than the NbTiN wire, but still the most sensitive SIS mixers for frequencies around 1 THz were made this way [3], [14], [15]. The reason for this is in heating of the junction once it is surrounded by the high-gap superconductors, making it difficult to sputter a high-quality NbTiN layer on the top of a deposited SiO_2 layer, which functions as an insulator in the micro-strip line.

To manufacture a sensitive SIS mixer operating in the 800–950 GHz atmospheric window [17], or even at higher frequencies, one needs to ensure that the NbTiN film is of the highest possible quality. More importantly, the properties of the film have to be tested not only by DC measurements, e.g. to determine the critical temperature, T_c, and its conductivity, σ, but by measuring the film performance at high frequencies, i.e. at the frequencies at which the mixer is operated. In addition, the tested NbTiN film should be of the same thickness as the one used in

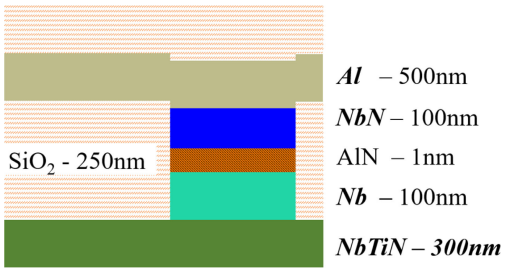

Fig. 1. Schematic representation of the layers used in SIS mixer [16] (not to scale). Here, the SIS junction is formed by Nb and NbN electrodes separated by AlN barrier, while Al and NbTiN layers form the embedding circuit - micro-strip line.

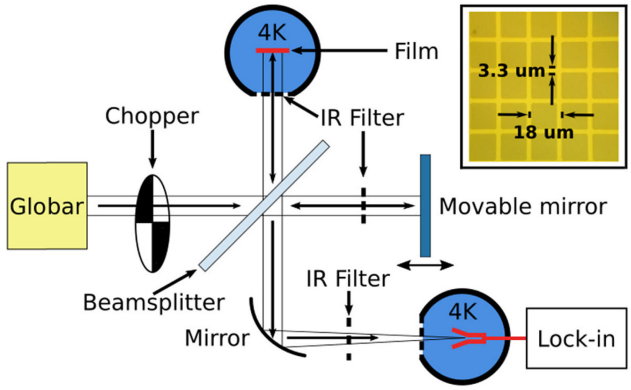

Fig. 2. Scheme of the Dispersive Fourier Transform Spectrometer. The wide-band signal form Globar is collimated and passes through chopper. Then the light enters the Fourier Transform Spectrometer consisting of 55 μm Mylar beamsplitter, movable mirror and the tested film (DUT) located in a cryostat and functioning as a stationary mirror. The signals reflected for the DUT and the mirror are combined after the beamsplitter and coupled to a wideband detector, which is connected with the chopper to a Lock-In.

the mixer, i.e. 300 nm or thicker, and its top surface should be probed. For that purpose we built a Dispersive Fourier Transform Spectrometer [18] (DFTS), which we used as a quality assurance tool of the NbTiN films and their manufacturing technologies. The scheme of DFTS and details of theoretical fit to the measurements of the NbTiN films are given in our recent paper [19]. Here, we will provide a summary of this work, and show the recently obtained experimental results. In addition to DFTS, we also used Time Domain Spectroscopy setup to verify the NbTiN film parameters, the results fo which are presented in this paper.

II. NbTiN Film Manufacturing

The tested NbTiN films were deposited by DC sputtering at room temperature using a NbTi target in a mixture of nitrogen and argon atmosphere [16].

The films were deposited on substrates of two different materials: silicon (Si) and fused quartz (Qu), and for both a solid and meshed films were made. The reason for testing quartz is because quartz is used in state-of-the-art SIS mixers with a NbTiN bottom electrode, since it provides a better match between the mixer antenna and the electromagnetic modes in the waveguide. At the same time, silicon substrates are cheaper and easier to use and, therefore, better suited for the optimization of technological processes by multiple depositions of different films.

We have tested two types of film structures: 1) solid film 2) meshed film. When square patched of the film are removed, a periodical mesh-type 2D pattern with a period of 18 μm and with a width of 3 μm is obtained. The mesh was fabricated using either reactive ion etching (RIE) process or lift-off. The motivation for the fabrication and testing of the meshed films is as follows, the technological processes utilized in fabrication of the SIS mixers involve different steps which can influence the quality of NbTiN bottom electrode due to contamination. For example, both lift-off and RIE are used to obtained the the shape of the NbTiN bottom wire. By fabrication and testing of the meshed films using DFTS we can directly check the effects that different technological processes have on the quality of the NbTiN films at high frequencies. In addition, the meshed film has lower effective conductivity and hence a lower reflection coefficient in the normal state. This gives a higher difference between reflection coefficient of the film in the normal and in the superconducting state, which is used in the measurements as explained in the following section.

The thickness of the deposited films are all close to 330 nm and the film area illuminated by the THz signal has 24 mm diameter.

The T_c's of the manufactured films were determined by DC measurements, and were all close to 14.6 ± 0.2 K. The DC conductivity in normal state at 15 K was $\sigma_{dc,cold} = 9.2 \pm 0.2 \times 10^5$ S/m, and the RRR of the films was measured to be very close to 1, as expected.

III. Dispersive Fourier Transform Spectrometer

A. DFTS Setup

To investigate the quality of thick NbTiN films by probing the top surface, we decided to use a Fourier Transform Spectrometer (FTS), which is based on Michelson interferometer, and we measured the signal reflected from the film. The idea is to measure the reflection of the film in two cases. First, in the superconducting state at a temperature of 5 K, and second, in the normal state at $T = 15\,K$, i.e. just above the critical temperature, T_c. The scheme of DFTS setup is shown in Fig. 2. Here, the Globar is used as wide-band source of THz radiation and a cryogenic bolometer with NEP of about $= 10^{-13}$ W$/\sqrt{\text{Hz}}$ [1] is used as a wide-band detector.

We replaced the stationary mirror of the FTS with the device under test, i.e. the NbTiN film. In the measured interferogram, we were able to distinguish between the reflection from the film and the reflection from the back side of the substrate (see Fig. 3). This enabled us to extract the signal reflected from the film plane only, removing any contributions from the back surface of the substrate and additional reflections in the setup.

In Fig. 3 it is shown the measured interferogram of the NbTiN film. The peak in the center corresponds to the film reflection, and around $x = -6$ mm we see the signal reflected from the back

[1] [Online]. Available: http://www.infraredlaboratories.com/Bolometers.html

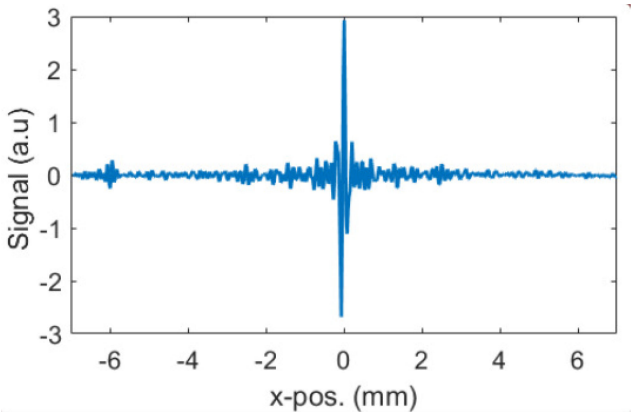

Fig. 3. Interferogram of NbTiN meshed film measured using the DFTS.

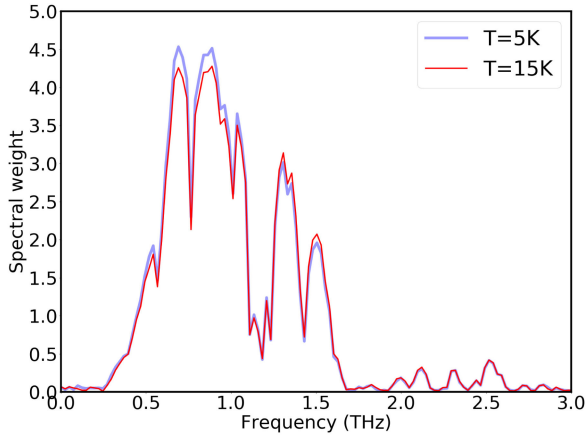

Fig. 4. DFTS spectra measured for the meshed NbTiN film in normal state at 15 K (dark curve) and in superconducting state at about 5 K (light curve). The zero spectral weight around 1.9 THz is the minimum in the periodic beamsplitter function. Strong absorption water lines are well seen at, for example, 1.2 THz.

side of the substrate. For this measurement, we added additional high-resistance silicon waivers to the back of the substrate, making the total thickness close to 1.8 mm. This allowed us to isolated the central part of the interferogram, i.e. in Fig. 3 $x = [-4\,mm, 4\,mm]$, and exclude the substrate back reflection. By taking the Fourier transform of the selected interferogram one gets a power spectrum with sufficient frequency resolution around 20 GHz, see Fig. 4.

This spectrum contains information on the reflection coefficient of the film, R. The intensity of the power spectrum is linearly proportional to the product of field amplitudes of each arm [20], i.e. to the square root of the film reflection coefficient R.

In Fig. 4 shows the DFTS power spectra measured for a meshed NbTiN film in the superconducting state ($T < T_c$) and the normal state ($T > T_c$). Here, one can already clearly see a higher power for the superconducting state at frequencies below 1 THz, i.e. below the gap frequency, and lower power at frequencies above 1.3 THz. In order to remove the spectral properties of the DFTS setup including the spectral functions of the detector, the source, the beamsplitter, and the water absorption lines, we take the normalised difference of these two

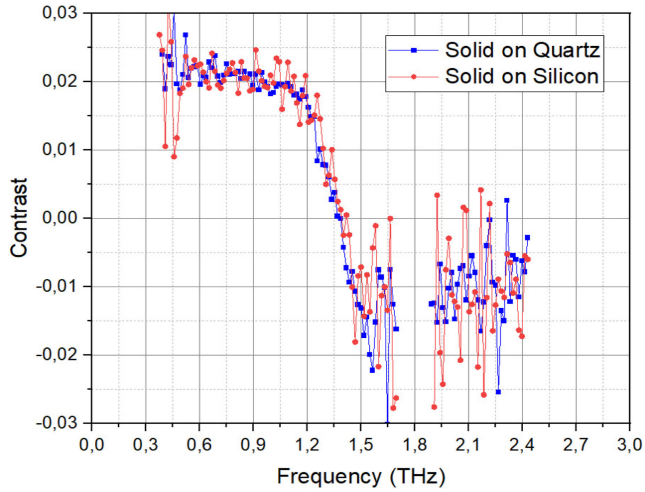

Fig. 5. Contrast curves measured for the solid NbTiN films sputtered on quartz (squares) and on silicon (circles) wafer.

spectra. This normalised difference is also called the contrast, $\tilde{S}$, which can be expressed by:

$$\tilde{S} = \frac{S_s - S_n}{S_n}. \tag{1}$$

Here, S_s and S_n are the power spectra taken for superconducting and normal state, respectively. The contrast can be used as a qualitative check to compare different films, and by fitting a theoretical model to the contrast we can extract the film parameters.

B. DFTS Experimetal Results

1) Contrast for Solid Films: Fig. 5 shows the contrast curves obtained for the solid NbTiN films of thickness 330 nm deposited in one technological circle on quartz and silicon substrates. The contrast curves are almost indistinguishable. This is an indication of equivalent quality of these films and makes it possible to use the silicon substrates for optimisation of the solid film technology with just a final check on quartz substrate. Theoretical fit described in the next Section III-C and in more details in [19], provides for these films the estimation of the energy gap of about $2\Delta/hc = 39\,cm^{-1}$, which corresponds to 1.17 THz in frequency.

2) Contrast for Meshed Films: Fig. 6 shows the contrast curves obtained for the meshed NbTiN films. Here, two films were sputtered in one technological run and the mesh structure was formed using the lift-off procedure. These films were about 360 nm thick. The third film was prepared separately with a smaller thickness of about 330 nm, and the meshed structure was etched using RIE process.

In case of the meshes films, it is much more difficult to determine their quality simply by looking at the contrast curve, because of dispersion introduced by the mesh structure. This dispersion also depends on the substrate properties, though, it is taken into account in the theoretical fit, and the obtained from the fit are objective. For the shown curves, the energy gap was found to be $2\Delta/hc = 37\,cm^{-1}$ and $41\,cm^{-1}$ for the lift-off on quartz

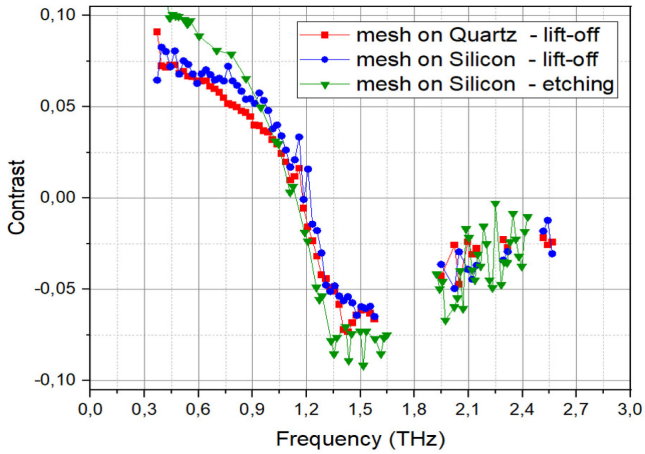

Fig. 6. Contrast curves measured for the meshed NbTiN films: Sputtered on quartz and formed by lift-off (squares); sputtered on silicon and formed by lift-off (circles); sputtered on silicon and formed by RIE (triangles).

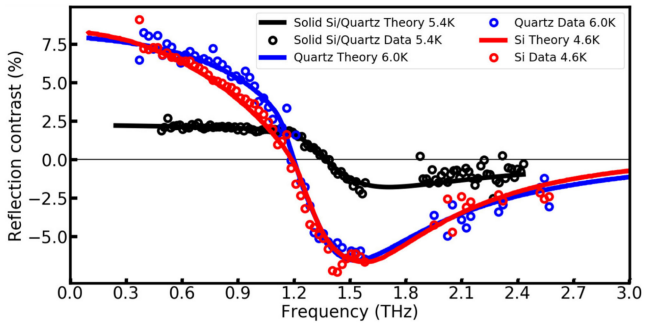

Fig. 7. Theoretical fit of some experimental contrast curves shown previously in Fig. 5 and 6. The fit is done for the solid film on silicon (black curve) and for the meshed films formed by lift-off process on quartz and silicon wafer.

and silicon, respectively, and 39 cm^{-1} for the RIE on silicon. This is a bit surprising result, because these numbers indicate that the quality of the meshed films on silicon is slightly better than the quality of the solid one. The difference is small, and stays almost within the measurement error, still it needs further investigation.

It is possible to make a direct comparison between the films deposited on silicon (see Fig. 6). Because of a smaller thickness, the contrast for the third film is a bit higher. Also, it is observed a small difference connected with the deviation in the obtained energy gap parameter. As a result, we conclude that both the lift-off and RIE provide more or less the same quality of the film with a bit of advantage of lift-off processing. For the pure comparison these films should be made in one technological run.

The obtained parameters of superconducting gap indicate that these films have good enough quality for manufacturing SIS mixers for frequencies up to 1 THz. Though, for producing the mixers around 1.2 THz this quality might be not sufficient.

C. Theoretical Fit of the Contrast Curve

The theoretical fit for the contrast curve is described in details in [19]. In short, the fit to the contrast curve of the solid film consisted of five steps. First, the normal state conductivity is calculated based on Drude model [21], [22]. Second, the superconducting state conductivity spectrum is calculated using Mattis-Bardeen theory [23] extended by including a complex gap parameter [24]. Third, the surface impedance of a solid film for both the superconducting and the normal state is calculated using the formula for thin film [24]–[26]. Fourth, the R is found by relating it to the surface impedance and the free-space impedance. Five, the contrast curve is calculated as a normalized difference of square roots of reflection coefficients for the superconducting and the normal state.

For the meshed film an 3D simulation (CST Microwave Studio) was used to calculate R of the meshed film knowing the parameters of the solid film, the geometrical parameters of the mesh, and the physical parameters of the substrate. The electromagnetic periodic structure of a single cell is exploited and modelled according to the Floquet theorem.

Fig. 7 shows the theoretical fits calculated for experimental data given earlier in Fig. 5 and in Fig. 6. Meshed films show clearly much higher contrast than the solid one. Here the fit is shown for the solid film on silicon and for the meshed films formed by lift-off process on quartz and silicon wafer.

IV. Time Domain Spectroscopy Measurements and Results

In addition to the measurements using a DFTS, we decided to test thick NbTiN films using Time Domain Spectroscopy. For this experiment we had to manufacture a separate set of NbTiN films - solid and a meshed one. Both films were deposited on silicon substrate in one technological circle. The NbTiN layer is 336 nm. The critical temperatures were found to be in between 14.1 and 14.6 K.

We used a Terahertz Time-Domain Spectrometer TeraView TPS 3000 to measure the spectra of the AC conductivity and conductance of the NbTiN layers in the normal and superconducting states. The conductivity and conductance spectra were determined basing on the transmission coefficient spectra of the film and meshed film on silicon substrate, see Fig. 8 and Fig. 9. The periodic oscillations seen in the spectra are due to multiple reflections of the radiation inside the plane-parallel silicon substrate. The transmissivity of the substrate decreases when it is covered with the investigated layers. In the normal state ($T > T_c$), the interferometric maxima of the spectrum have equal amplitudes, while noticeable dispersion is seen in the spectrum of the mesh, which is caused by its structured geometry. The transition of the NbTiN material into a superconducting state leads to a strong changes in the spectra of both samples, and they acquire a typical shape that is due to emergence of a superconducting energy gap in the density of states of the material [27]–[29]. Least-square modelling of the measured spectra with the standard Fresnel expression (see, ex., [30]) for transmission coefficient of a two-layered system (substrate+film) allowed us to determine electrodynamic parameters of the films in both the normal and superconducting states (properties of bare silicon substrate were determined separately beforehand).

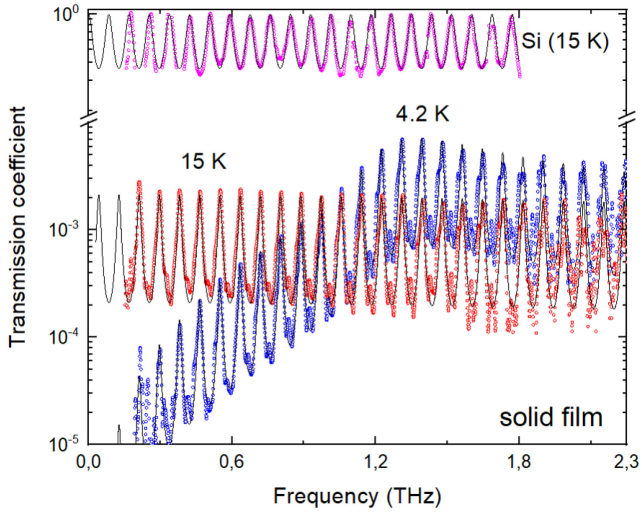

Fig. 8. Terahertz spectra of transmission coefficient of silicon substrate (Si) measured at T=15 K and of NbTiN film on Si substrate measured at $T = 15K > T_c$ and $T = 4.2\,K < T_c$. The dots indicate the experimental data, and the solid lines represent least-square fit results, as described in the text.

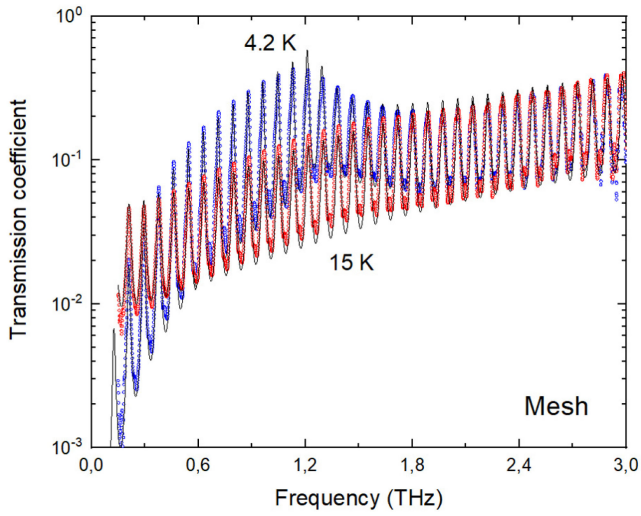

Fig. 9. THz spectra of transmission coefficient of NbTiN meshed film on Si substrate measured at $T = 15K > T_c$ and $T = 4.2\,K < T_c$. The dots are the experimental data, and the solid lines represent least-square fit results, as described in the text.

The normal-state properties of the bulk NbTiN film were modelled with the standard Drude expression for complex conductivity $\sigma* = \sigma_0(1 - i\omega\tau)^{-1}$ [31], [32], where σ_0 is the DC conductivity, ω is angular frequency, $\tau = (2\pi\gamma)^{-1}$ is the scattering time and γ is the scattering rate. At $T = 15\,K$ we obtained $\sigma_0 = 10.7 \times 10^5 S/m$ and $\gamma = 246\,cm^{-1}$. The geometrical boundaries of the meshed film cannot be specified precisely, therefore we analyzed its response without assigning a thickness to the film and without specifying its structure. Here, we use the model for complex conducting surfaces developed in [33], and we express the real part of the mesh conductance as σd, where σ is the real part of the conductivity and d is the thickness of the film if it were homogeneous. For the meshed film in the

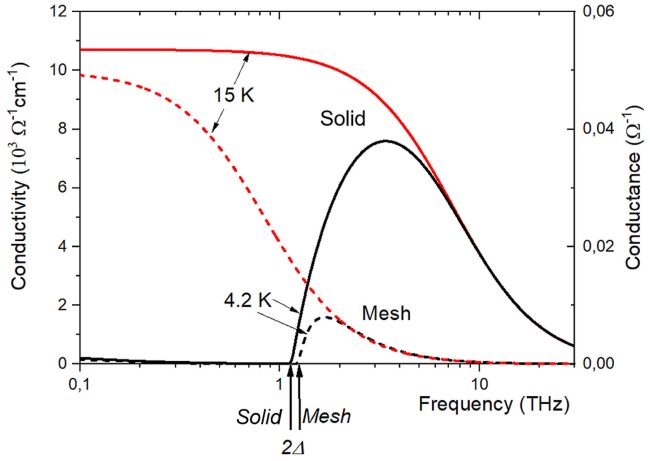

Fig. 10. Terahertz spectra of AC conductivity of solid NbTiN film (solid lines) and of conductance of NbTiN meshed film (dashed lines) measured at $T = 15K > T_c$ and $T = 4.2\,K < T_c$ (marked by text and arrows). The values of superconducting energy gap 2Δ are indicated by arrows at the X-axis.

normal state we obtain σd=0.05 S and $\gamma = 28\,cm^{-1}$, which together characterize the effective charge dynamics in the meshed structure. In the superconducting state, the complex conductivity of the samples is described according to the Mattis-Bardeen theory [23], see Fig. 10 for the results. The conductivity spectrum of the film has a shape that is typical for metals, i.e. a slight frequency dependence is seen for $\nu << \gamma$, but which decreases strongly at $\nu \approx \gamma$. Sharp threshold at $38\,cm^{-1}$ in the spectrum measured at $T = 4.2\,K$ indicates the presence of the superconducting gap [27]–[29] $2\Delta(4.2\,K) = 4.71meV \pm 0.25meV$ and $2\Delta/k_BT_c = 4.0$ indicating the strong-coupling case (here k_B is the Boltzman constant). Although the quantitative characteristics of the meshed film should be considered as effective, the kink at $41\,cm^{-1}$ in the conductance spectra corresponds to an energy gap of $2\Delta(4.2\,K) = 5.08$meV$\pm$0.25 meV. The values of energy gaps for the solid and meshed films are very close and coincide within the experimental uncertainty. At the same time, there is an indication of a slightly higher energy gap for the meshed film, which is surprising and needs further investigation.

V. Conclusion

We have performed test measurements of bulk and meshed NbTiN films deposited on dielectric substrates at terahertz frequencies using the techniques of dispersive Fourier-transform spectroscopy (DFTS) and a time-domain spectroscopy (TDS). Both techniques allow for determination of the superconducting energy gap with a high precision and can be used to control the terahertz electrodynamic properties of superconducting films. TDS has clearly a higher potential, because it provides better signal-to-noise ratio for the measured transmission spectra, as compared with the reflectivity spectra provided by the DFTS. At the same time, both approaches give the same uncertainty of about a few percent in determining the superconducting energy gap value. Although the two techniques employed measurements of different NbTiN films, both samples were manufactured using identical recipes, which ensures the validity of the

conclusions drawn. Further comparative studies of the possibilities of both methods in relation to the study of superconducting films are in progress.

A future application of the presented DFTS and TDS schemes is to test the top electrode of the embedding circuit. In this case, the NbTiN film should be deposited on the top of 250-300 nm quartz layer sputtered earlier on the wafer. In case of DFTS, the transmissivity measurement should be performed through the substrate to probe exactly the surface, which would operate in the micro-strip line.

ACKNOWLEDGMENT

The authors would like to acknowledge Prof. A. A. Golubov for helpful discussions on theoretical models to fit the experimental data.

REFERENCES

[1] A. R. Kerr *et al.*, "Development of the ALMA band-3 and band-6 sideband-separating SIS mixers," *IEEE Trans. THz Sci. Technol.*, vol. 4, no. 2, pp. 201–212, Mar. 2014.

[2] A. M. Baryshev *et al.*, "The ALMA band 9 receiver–Design, construction, characterization, and first light," *Astron. Astrophys.*, vol. 577, May 2015, Art. no. A129.

[3] T. De Graauw *et al.*, "The Herschel-heterodyne instrument for the far-infrared (HIFI)," *Astron. Astrophys.*, vol. 518, 2010, Art. no. L6.

[4] "ALMA observatory," [Online]. Available: http://www.almaobservatory.org

[5] J. Chenu *et al.*, "The front-end of the NOEMA interferometer," *IEEE Trans. THz Sci. Technol.*, vol. 6, no. 2, pp. 223–237, Mar. 2016.

[6] R. Güsten *et al.*, "APEX: The Atacama Pathfinder EXperiment," in *Ground-Based and Airborne Telescopes*, L. M. Stepp, Ed., vol. 6267, Bellingham, WA, USA: SPIE, 2006, pp. 389–414.

[7] "The submillimeter array," [Online]. Available: https://www.cfa.harvard.edu/sma/

[8] "The Greenland telescope," [Online]. Available: https://www.cfa.harvard.edu/greenland12m/

[9] "Millimetron Space Observatory," [Online]. Available: https://millimetron.ru/en/

[10] G. Bubnov *et al.*, "The results of astroclimate observations in the short-wave length interval of the millimeter-wave range on the Suffa plateau," *Radiophys. Quantum Electron.*, vol. 59, no. 8/9, pp. 763–771, 2017.

[11] "Atacama large aperture submillimeter telescope project," [Online]. Available: https://www.atlast.uio.no/

[12] J. R. Lépine *et al.*, "The LLAMA Brazilian-Argentinian radiotelescope project: Progress in Brazil and BRICS collaboration," *Anais da Academia Brasileira de Ciências*, vol. 93, 2021.

[13] J. R. Tucker and M. J. Feldman, "Quantum detection at millimeter wavelengths," *Rev. Modern Phys.*, vol. 57, no. 4, 1985, Art. no. 1055.

[14] Y. Uzawa *et al.*, "Development and testing of band 10 receivers for the ALMA project," *Physica C, Supercond.*, vol. 494, pp. 189–194, 2013.

[15] M. Kroug, T. Kojima, Y. Fujii, K. Ohtawara, A. Miyachi, and Y. Uzawa, "Noise performance of ALMA band 10 receivers employing high-JC SIS mixers," in *Proc. 29th IEEE Int. Symp. Space THz Technol.*, 2018.

[16] A. Khudchenko *et al.*, "High-gap Nb-AlN-NbN SIS junctions for frequency band 790–950 GHz," *IEEE Trans. THz Sci. Technol.*, vol. 6, no. 1, pp. 127–132, Jan. 2016.

[17] [Online]. Available: http://www.apex-telescope.org/weather/

[18] J. Birch, "Dispersive Fourier transform spectroscopy," *Microchimica Acta*, vol. 93, pp. 105–122, Jan. 1987.

[19] B. Lap *et al.*, "Characterization of superconducting NbTin films using a dispersive fourier transform spectrometer," *Appl. Phys. Lett.*, vol. 119, no. 15, 2021, Art. no. 152601.

[20] S. P. Davis, M. C. Abrams, and J. W. Brault, *Fourier Transform Spectrometry*. Amsterdam, The Netherlands: Elsevier, 2001.

[21] N. W. Ashcroft and N. D. Mermin, *Solid State Physics*. Brooks/Cole Cengage Learn. Learn., 1976.

[22] J. Lloyd-Hughes and T.-I. Jeon, "A review of the terahertz conductivity of bulk and nano-materials," *Int. J. Infrared Mil. Waves*, vol. 33, pp. 871–925, Sep. 2012.

[23] D. C. Mattis and J. Bardeen, "Theory of the anomalous skin effect in normal and superconducting metals," *Phys. Rev.*, vol. 111, pp. 412–417, 1958.

[24] T. Noguchi, M. Naruse, and Y. Sekimoto, "RF conductivity and surface impedance of a superconductor taking into account the complex superconducting gap energy," *Phys. Procedia*, vol. 36, pp. 318–323, 2012.

[25] P. Hartemann, "Effective and intrinsic surface impedances of high-T/sub c/ superconducting thin films," *IEEE Trans. Appl. Supercond.*, vol. 2, no. 4, pp. 228–235, Dec. 1992.

[26] J. C. Booth, D. H. Wu, and S. M. Anlage, "A broadband method for the measurement of the surface impedance of thin films at microwave frequencies," *Rev. Sci. Instrum.*, vol. 65, no. 6, pp. 2082–2090, 1994.

[27] B. Gorshunov *et al.*, "Terahertz BWO-spectrosopy," *Int. J. Infrared Millimeter Waves*, vol. 26, no. 9, pp. 1217–1240, 2005.

[28] R. Glover III and M. Tinkham, "Conductivity of superconducting films for photon energies between 0.3 and 4 0 k T C," *Phys. Rev.*, vol. 108, no. 2, 1957, Art. no. 243.

[29] D. M. Ginsberg and M. Tinkham, "Far infrared transmission through superconducting films," *Phys. Rev.*, vol. 118, no. 4, 1960, Art. no. 990.

[30] M. Born and E. Wolf, *Principles of Optics*. 1999, ch. 1.

[31] A. Sokolov, *Optical Properties of Metals*, vol. 22. New York, NY, USA: Elsevier, 1967, p. 472.

[32] M. Dressel and G. Grüner, *Electrodynamics of Solids*. Cambridge, U.K.: Cambridge Univ. Press, 2002.

[33] Y. Troitskii, "Dispersed metallic films," *Dispersed Metallic Films. Kiev, Inst. Phys. USSR Acad. Sci.*, 1972.